Journal of Thermal Analysis and Calorimetry (2023) 148:6035–6045
https://doi.org/10.1007/s10973-023-12172-7

Effect of heat treatment temperature and atmosphere on physiochemical properties and oxidation behaviour of a Chinese lignite

Xiaofei Long[1] · Jianbo Li[1] · Jiarui Yuan[1] · Xiuqi Shu[1] · Xiaofeng Lu[1]

Received: 16 August 2022 / Accepted: 4 April 2023 / Published online: 20 April 2023

Abstract
This work investigates how heat treatment temperature and atmosphere would affect the physicochemical properties and oxidation behaviour of Zhundong lignite (ZD). Samples of ZD were firstly heated at 150–400 °C in either N_2 or simulated flue gas (FG) atmosphere, which were then analysed to obtain their mass losses, elemental composition, oxygen-containing functional groups (OCFGs) and water re-adsorption capacities. Results showed that the dried ZD subjecting to N_2 atmosphere had a mass loss of 9.90 mass%–10.95 mass% at 150–250 °C, but further increased to 25.17 mass% at 400 °C, leading to an increase in C/O ratios from 2.49 to 4.70 as treatment temperature increased. FTIR analysis revealed that OCFGs including hydroxyl, carboxyl, carbonyl and ether bond decreased as heat treatment temperature increased, which also deceased the water re-absorption capacity of heat-treated ZDs. While it is heated in FG, the mass loss of ZDs at temperatures below 300 °C was roughly equivalent to those in N_2, but was less than those at 350–400 °C, due to the incorporation of O along with increased OCFGs peak intensities at these temperatures. This also allowed for the re-absorption of more moisture than those samples treated in N_2. In addition, the combustion reactivity of the heat-treated ZDs was enhanced and the combustion process turned into higher temperature zone with increasing treatment temperature, suggesting that the variation in physicochemical properties of heat-treated ZDs also affected their oxidation behaviour.

Keywords Lignite upgrading · Physicochemical properties · OCFG · Oxidation behaviour · Zhundong lignite

Introduction

Although "carbon peak" and "carbon neutral" have attracted a great deal of attention, coal still plays an important role be in China and other developing countries [1], at least in a short term. Clean and efficient utilisation of coal is therefore mandatory so that CO_2 is to be released as less as possible. Regarding the coal resources, lignite has an estimated worldwide reserve of 860,938 Million tons [2] and accounts for 13% of the overall coal recourses in China. For instance, the Zhundong lignite alone is predicted to have a reserve of 390 billion tons and would provide 100-year energy supply for China [3, 4]. However, lignite is often characterised by high moisture and high volatile matter (VM) contents [5, 6]. The abundance of moisture in lignite would not only increase the cost for long-distance transportation [7], but also decrease the overall efficiency and correspondingly increase the CO_2 emission during combustion [8]. The high VM in lignite, likewise, would increase its tendency for spontaneous combustion, raising its risk for storage [9]. Reducing the moisture and/or VM contents is therefore considered as an essential process prior to its subsequent utilisation.

Among the various means that reported in the literature, heat (or thermal) treatment is an essential pre-treatment process to reduce the moisture and VM contents in lignite. This often includes but not limited to heating the lignite in hot air, combustion gases, superheated steam, hydrothermal processing and even in microwave [10–12]. It has been proved that the heat-treated lignite following the above methods would reduce its moisture content, increase its calorific value and lessen its propensity for spontaneous combustion [5, 13]. Fundamentally, it is the underlining changes in physicochemical properties of lignite, including collapse or

✉ Jianbo Li
Jianbo.li@cqu.edu.cn

[1] Key Laboratory of Low-Grade Energy Utilization Technologies and Systems, Ministry of Education of PR China, Chongqing University, 174 Shapingba Main street, Chongqing 400044, China

shrinkage of pore structure, evolution of oxygen-containing functional groups (OCFGs) and chemical composition that account [14–16]. For instance, Hulston J et al. [17] found that heat treatment would induce collapse of macro-pores and formation of meso-pores on coal surface, therefore squeezing water from pores [18]. Meanwhile, Salmas CE et al. [19] found that heat treatment of lignite by steam would stimulate the shrinkage of particle size along with the irreversible change of pore structure [4, 5]. Likewise, Feng X et al. [20] found that thermal treatment of Zhaotong lignite facilitated the loss of moisture and oxygen content at temperature 150–300 °C. As for OCFGs, the main OCFGs in lignite include carboxyl group (COOH), phenolic hydroxyl group (Ar-OH), carbonyl group (C = O), methoxyl group (OCH_3) and ether bond (-O-), some of which are highly hydrophilicity and tend to bond with moisture [12, 21]. During heat treatment, decomposition of unstable functional groups and a simultaneous oxidation of aliphatic groups would occur. For instance, peroxides and hydroperoxides begin to be oxidised at temperatures as low as 50 °C [22]. Carboxyl and methoxyl groups would decompose to small molecules including CO_2 at temperature higher than 160 °C, while carbonyl groups are relatively stable at temperatures no more than 200 °C [13, 21]. The phenolic hydroxyl group would remain stable at 240 °C and below, but would be decreased as temperature further increased. However, the overall functional groups might not change significantly at temperatures below 300 °C [23]. Moreover, the changes in physicochemical properties of lignite during heat treatment are also dependent on heating medium [10], i.e., flue gas, air, nitrogen or steam, leading to the differences in OCFGs once heated [7, 12]. For instance, a decrease in OCFGs as temperature was observed when N_2 or steam was used as the heating medium [24], while an increase in OCFGs was found in the presence of O_2 due to the oxidation reactions of aliphatic in the organic structure [7, 14]. In particular, the use of flue gas as the heating medium could not only upgrade lignite in conventional powder stations, but also recover the waste heat in flue gas [19]. However, the effect of temperature and flue gas during heat treatment on physiochemical properties of Zhundong lignite has rarely been reported.

The heat-treated lignite is also found to re-absorb moisture due to the presence of OCFGs and micro- or meso-pores [20, 25]. OCFGs including hydroxyl, carboxy and carbonyl groups are reported to have strong hydrophilicity [26] and are prone to bound with water molecule through hydrogen bonds [4], and form non-freezable water. Provided these OCFGs are decomposed, the water re-adsorption ability of heat-treated lignite would be decreased [27]. In addition, the water molecule might bond together and form freezable water in the micro- or meso-pores [2]. The collapse of porosity is therefore reported to weaken its water re-adsorption ability [4], due to the shrinkage of particles and colloidal gel of lignite [28]. However, the re-absorption characteristics of heat-treated Zhundong lignite have not been examined.

Besides, the combustion performance of the heat-treated lignite is also varied due to the physicochemical variations upon heat treatment [2, 15, 29]. Researchers including Zhao P, Zhao H and Sun M have investigated the thermal oxidation behaviour of the heat-treated Shengli lignite, Xilingou lignite and a bituminous coal [10, 13, 30]. It has been found that the burnout temperature of the heat-treated lignite was increased with treatment temperature [10, 31]. This might be attributed to the crystalline structure ordering representing the oxidation reactivity since it becomes more stable at higher heat treatment temperature [8]. Meanwhile, the specific surface area is found decreased with increasing heat treatment temperature [21], weakening the oxygen adsorption ability of heat-treated lignite as a consequence [26]. In addition, the OCFGs would provide active sites for oxygen and the variation in OCFGs would inevitably affect its combustion reactivity [26, 32]. However, the oxidation behaviour of Zhundong lignite after heat treatment has not so far been reported.

This paper therefore presents an experimental investigation into the physiochemical evolutions of Zhundong lignite upon heat treatment in N_2 and simulated flue gas atmosphere at temperatures 150–400 °C. Elemental composition, particle size distribution, special surface area, OCFGs and re-absorption characteristics of the samples heat-treated in both atmospheres were characterised in detail and their oxidation characteristics was studied as well. The outcome of this study is expected to provide a better comprehension on the physicochemical properties and combustion characteristics of the heat-treated Zhundong lignite and provide basic data for heat treatment of the Zhundong lignite in industrial practice.

Experimental

Materials

The "run-of-mine" Zhundong lignite (ZD) from Northwest China was used as the experimental material. It was crushed and sieved into particles within 200 μm in size prior to analysis, in accordance with the Chinese standard GB/T 212–2008. Proximate and ultimate analysis of ZD and the chemistry of its ash prepared in a muffle furnace in air at 550 °C are listed in Table 1. It is seen that the as-received ZD has a moisture content of 24.58 mass% and a volatile matter of 23.16 mass%. These are the typical features of the lignite [33]. Meanwhile, the O content in the dried ZD is 24.69 mass%, which might be attributed to the presence of OCFGs such as hydroxyl, carboxyl and carbonyl functional groups [3]. With respect to ash chemistry, the ash from ZD

Table 1 Proximate, ultimate analysis of ZD and the chemical composition of its ash

Sample	Ultimate analysis/mass%, dry					Proximate analysis/mass%, dry				$Q_{ar.net}$
	C	H	O	N	S	M_{ar}	V_{ar}	A_{ar}	FC_{ar}	kJ/kg
ZD	65.45	3.51	24.69	0.69	0.57	24.58	23.16	2.91	48.90	21,660
	SiO_2	Al_2O_3	Fe_2O_3	CaO	MgO	TiO_2	SO_3	P_2O_5	K_2O	Na_2O
Ash chemistry	11.71	6.69	5.93	32.50	7.56	0.39	27.93	0.09	0.44	4.90

is as low as 2.91 mass%, but riches in CaO (32.50 mass%) and Na_2O (4.90 mass%).

Heat treatment and moisture re-adsorption

The as-received ZD was firstly dried in an oven at 105 °C in air for 2 h to obtain the dried ZD. Furthermore, the dried ZD of about 2 g was then loaded into an alumina crucible, placed into a fixed-bed reactor (Fig. 1) and heated there at 150, 200, 250, 300, 350 and 400 °C, respectively, for 2 h, with N_2 or simulated flue gas (FG) comprising 12% CO_2, 6% O_2 and 82% N_2 being the heat treatment atmosphere. These samples were then retrieved from the reactor, cooled down to room temperature under N_2 and stored in a desiccator.

To obtain their water re-adsorption characteristics, the heat-treated samples of about 20 mg was spread evenly on a crucible and placed into a chamber at constant temperature of 25 °C and relative humidity of 65% for 72 h. The samples were then weighted within the set time to obtain their mass changes as a function of time.

Analysis and Characterisation

A Unicube elemental analyser was used to obtain the elemental contents of C, H, N and S of dried or heat-treated ZD in accordance with GB/T 31391-2015 standard. Meanwhile, a BT-9300HT laser particle size analyser was used to analyse the size distribution of these samples. Each analysis was repeated three times, and the relative error of the analyser was within 5%.

To analyse the OCFGs, these samples were firstly mixed and ground in an agate mortar with spectroscopic-grade KBr at 1:400 ratio for 10 min. The mixture was then pressed to a disc at a pressure of 10 MPa and analysed by A Nicolet iS50 Fourier transform infrared spectroscopy (FTIR) with pure KBr disc as the reference spectrum. The spectra were obtained with 32 scans over the scope of 500-4000 cm^{-1} wave numbers at a resolution of 4 cm^{-1}. Quantitative composition of the OCFGs was obtained by peak fittings using the existing analytical method as reported in the literature [32]. A typical fitting curve versus the actual spectra is shown in Fig. 2.

In addition, A STA 409 PC/PG Luxx® thermogravimetric analyser (TGA) was used to analyse the oxidation behaviour of these samples. Dried ZD or samples heat-treated in FG of about 10 mg was firstly placed into the crucible, which was then heated in TGA from ambient temperature to 950 °C at a heating rate of 20 °C min^{-1} in 100 mL min^{-1} air. The combustion behaviour of the dried ZD at this single heating rate could therefore be obtained, since the effect of heating rate might be quite limited [34]. In addition, to evaluate the combustion characteristics of these samples, the flammability index (FI) and comprehensive combustion index (CCI), as follows, were defined [31, 34].

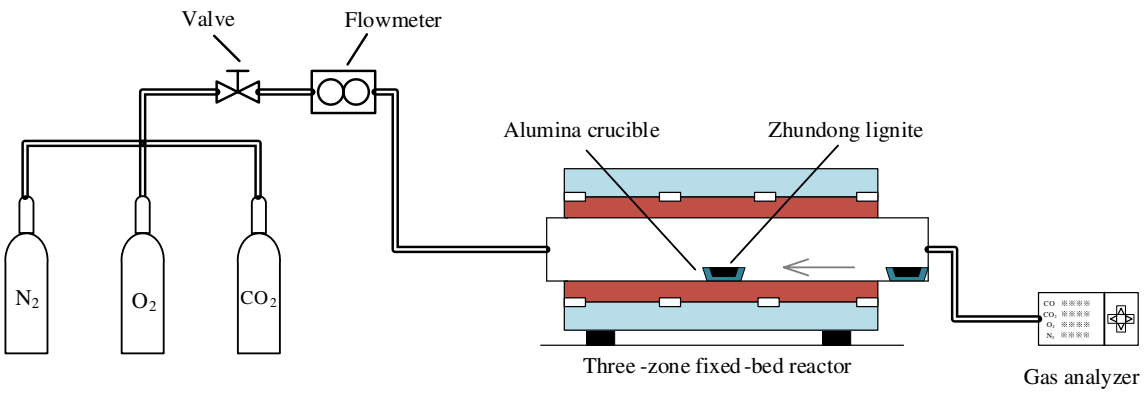

Fig. 1 Schematic diagram of the fixed-bed reactor

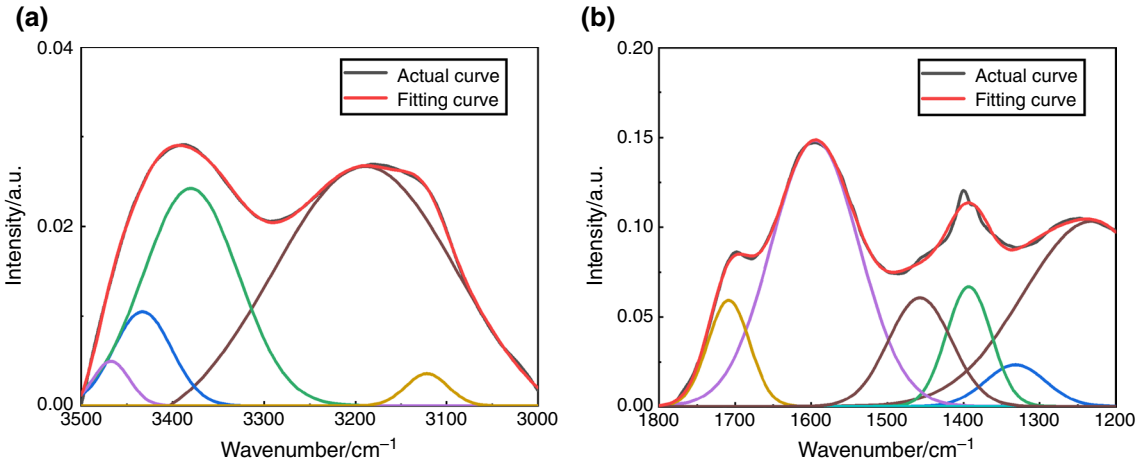

Fig. 2 Curve-fitted spectra of the 3500–3000 cm^{-1} and 1800–1200 cm^{-1} for dried ZD

$$FI = \frac{DTG_{max}}{T_i T_p} \quad (1)$$

$$CCI = \frac{DTG_{max} DTG_{mean}}{T_i^2 T_b} \quad (2)$$

among which T_i is ignition temperature computed by intersection method [10, 35], T_b is the burnout temperature estimated by the conversion method (98% conversion of the fuel), T_p is the temperature with the maximum mass loss, DTG_{max} is the maximum mass loss and DTG_{mean} is the average maximum mass loss. Noteworthy that the combustion behaviour of these samples subjecting to different heating rates might require further and comprehensive investigation, but is outside the scope of this study.

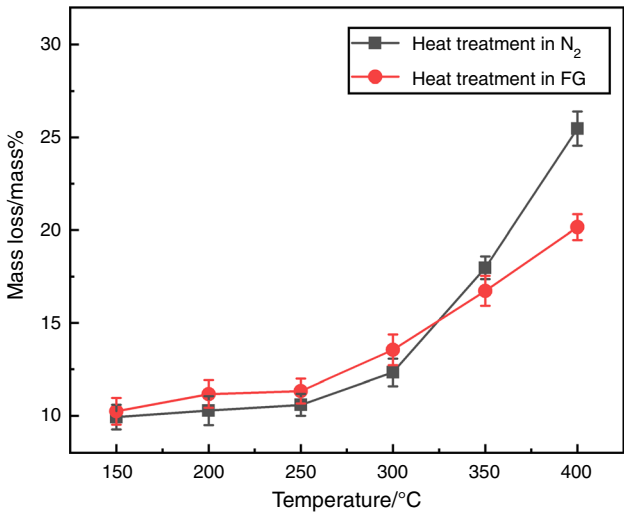

Fig. 3 Mass loss of heat-treated ZDs in N_2 and FG at 150–400 °C

Results and discussion

Mass loss as temperature and atmosphere

The mass loss during heat treatment at 150–400 °C in both N_2 and FG is illustrated in Fig. 3. With the dried ZD as the basis, the mass loss of ZD at 150 °C in N_2 was 9.93 mass%, indicating that a portion of water mainly inherent water was indeed presented in ZD even if it has been dried at 105 °C. As temperature increased to 250 °C, the mass loss increased merely to 10.59 mass%, but a further increase in temperature to 300, 350 and 400 °C resulted in a mass loss of 12.33 mass%, 17.97 mass% and 25.47 mass%. This suggests that the mass loss of ZDs below 250 °C was mostly due to the release of moisture, while the extra mass loss of ZD above 250 °C was attributed to the release of VM [13, 21, 22]. Likewise, the mass loss of ZD in FG atmosphere increased from 10.25 mass% at 150 °C to 11.17 mass% at 200 °C, 11.33 mass% at 250 °C, 13.54 mass% at 300 °C, 16.73 mass% at 350 °C and 20.16 mass% at 400 °C. This suggests that heat treatment in FG at temperature above 250 °C would lead to the release of VM and possibly also the change of coal structure. In addition, the mass loss of ZD below 300 °C in FG was always higher than those heat-treated in N_2. This is because heat treatment in FG would provide available O_2 and CO_2 for oxidation of VM and promote the mass loss. However, at temperatures above 350 °C, the mass loss in FG was lower than that in N_2. This is because heat treatment in FG at these temperatures would not only allow for the release of VM, but also promote absorption of oxygen [10], leading to a lessened mass loss. Detailed evidences are provided in Sect. "Evolution of OCFGs."

Chemistry and particle size variation

Elemental compositions (C, H, O, N and S) of these samples were also analysed and the results are shown in Table 2. Herein the C and O contents were discussed for simplicity. The 105 °C dried ZD had a C content of 67.88 mass%. As heated in N_2, C content of heat-treated ZDs increased to 72.44 mass% at 250 °C, to 78.06 mass% at 350 °C and to 78.71 mass% at 400 °C. This implies that the C content in heat-treated ZD increased as temperature increased. Correspondingly, the O content decreased from 27.23 mass% to 22.48 mass% at 105–250 °C and reached 16.73 mass% at 400 °C, showing a moderate decrease between 105 and 250 °C and a sharp decrease above 300 °C. The ratio of C/O thus decreased from 2.49 to 4.70 as a function of heat treatment temperature. The release of moisture and VM would be responsible for this variation [12, 25], since oxygen in water and volatile matter would be removed as OCFGs were dissolved [4, 14]. However, with FG being the heat treatment atmosphere, the C content increased initially to 76.75 mass% at 300 °C, but decreased afterwards to 69.34 mass% at 350 °C and to 66.02 mass% at 400 °C. The O content therefore increased to 29.02 mass% and even overweighed that in dried ZD. The ratio of C/O increased firstly at heat temperatures below 300 °C, but decreased to 2.65 and 2.67 at 350–400 °C. This differed from those treated in N_2 in which an increase in C/O ratio were always observed. In FG with the presence of CO_2, N_2 and O_2, evolution of OCFGs and moderate oxidation of carbon would occur, decreasing C content but also allowing for absorption of O into the heat-treated ZDs [14, 15].

For their particle sizes as shown in Table 3, the mean particle size (D_{50}) of dried ZD was 108.3 µm. As temperature increased to 250 °C, D_{50} of heat-treated ZDs in N_2 decreased to 87.54 µm, but increased to 109.9 µm as temperature further raised to 400 °C. This is because the release of moisture between 150 and 250 °C would affect the coal structure and decrease their sizes [3, 4, 16]. However, at higher temperatures, reforming of coal structure and coalescence or condensation of VM might occur [36], increasing the particle size as a consequence. Likewise in FG atmosphere, the particle sizes of heat-treated ZDs decreased at temperatures below 250 °C, but increased afterwards once the heat treatment temperature elevated further. As for their specific surface areas, the BET specific surface area of dried ZD was 4.29m^2g^{-1}, while those of heat-treated ZDs in N_2 and FG decreased to 2.89 m^2g^{-1} and 2.76 m^2g^{-1} at 400 °C. This is in accordance with their particle size distribution and also consistent with these reported [21, 37]. The collapse of macro-spores and

Table 3 D_{50} and BET special surface area of dried ZD and heat-treated ZDs

Samples	D_{50}/µm	BET/ $m^2 \cdot g^{-1}$	Samples	D_{50}/µm	BET/$m^2 \cdot g^{-1}$
Dried ZD	108.3	4.29			
150 °C–N_2	96.56	4.18	150°C_FG	90.01	4.15
200 °C–N_2	91.43	4.10	200°C_FG	87.15	3.97
250 °C–N_2	87.54	3.95	250°C_FG	86.28	3.64
300 °C–N_2	90.52	3.49	300°C_FG	89.66	3.34
350 °C–N_2	104.8	3.13	350°C_FG	98.34	3.08
400 °C–N_2	109.9	2.89	400°C_FG	104.9	2.76

Table 2 Ultimate analysis of dried ZD and samples treated in N_2 and FG at 105–400 °C

Samples	Ultimate analysis/mass%, dry and ash free					
	C	H	N	S	O	C/O
Dried ZD	67.88	3.74	0.57	0.57	27.23	2.49
150 °C-N_2	70.50	4.03	0.84	0.62	24.01	2.94
200 °C-N_2	70.54	3.54	0.56	0.57	24.79	2.85
250 °C-N_2	72.44	3.79	0.67	0.62	22.48	3.22
300 °C-N_2	73.05	3.57	0.64	0.63	22.10	3.31
350 °C-N_2	78.06	3.75	0.64	0.70	16.86	4.63
400 °C-N_2	78.71	3.33	0.53	0.70	16.73	4.70
150 °C-FG	71.13	3.93	0.58	0.64	23.72	3.00
200 °C-FG	73.75	3.17	0.88	0.78	21.42	3.44
250 °C-FG	76.57	3.63	0.74	0.74	18.30	4.18
300 °C-FG	76.75	3.47	0.76	0.71	18.32	4.19
350 °C-FG	69.34	3.25	0.57	0.63	26.21	2.65
400 °C-FG	66.02	3.49	0.85	0.62	29.02	2.27

The ash content was determined as 3.86% in dry basis; O is determined by difference

formation of meso-pores would play a non-negligible role for the changes of the specific surface area [4].

Evolution of OCFGs

Figure 4 presents the FTIR spectra of heat-treated ZDs in N_2 and FG atmosphere at 105–400 °C, and the referred band assignments are listed in Table 4. For dried ZD, the peaks at 3748–3688 cm^{-1} are related to free hydroxyl group (3748–3726 cm^{-1}) and stretching vibrations of O–H (3705–3688 cm^{-1}). The peaks centred around 3432–3365 and 3152–3132 cm^{-1} are related to –OH bond within phenolic/alcohol. The peaks at 2851 and 2919–2913 cm^{-1} correspond to symmetric or asymmetric stretching of CH_2. Meanwhile, OCFGs (1800–1200 cm^{-1}) and aliphatic group including carboxyl groups (1708 cm^{-1}), stretching vibration of C = C (1600 cm^{-1}), asymmetric $–CH_3$ and $–CH_2$ (1458 cm^{-1}), stretching vibration of $–CH_3$ (1398 cm^{-1}), symmetric $CH_2 – C{=}O$ (1350 cm^{-1}) and stretching vibration of C–O (1225–1186 cm^{-1}) are also observed. In addition, the FTIR peak at 1126 cm^{-1} represents C–O–C aliphatic ether, and the peak at 757 ~ 748 cm^{-1} refers to out-of-plane deformation vibration of aromatic = C–H in aromatic structures. The peak at 669 cm^{-1} corresponds to substituted benzenes.

For heat-treated ZDs, the changes of FTIR peaks occurred mainly in the region of 3500–3000 cm^{-1} and 1800–1200 cm^{-1}, indicating that the hydroxyl group and OCFGs had been changed [15]. To quantify the changes in OCFGs, fitting of the FTIR peaks was done and the results are shown in Fig. 5. As shown in Fig. 5a, the fitted peak areas of ether bond, carboxyl, carbonyl and hydroxyl were 14.9, 5.2, 2.1 and 10.2 for dried ZD, but the areas of these peaks decreased from 12.5, 4.00, 1.95 and 9.8, respectively, at 150 °C to 8.86, 1.71, 1.25 and 7.30 at 250 °C, indicating

Table 4 Band assignments in the FTIR spectra of samples

Serial number	Wave number/cm^{-1}	Assignment [3, 14, 21, 39, 40]
1	3748–3726	Free hydroxyl group
2	3705–3688	Stretching vibration of –OH
3	3432–3365, 3152–3132	–OH bond in phenolic/alcohol
4	2919–2913, 2851	Stretching of CH_2
5	1708	C = O in carboxylic group
6	1600	Stretching vibration of C = C
7	1458	Asymmetric $–CH_3$ and $–CH_2$
8	1398	Stretching vibration of $-CH_3$
9	1350	Symmetric $CH_2 – C{=}O$
10	1225–1186	C-O in phenolic group
11	1126	C–O–C aliphatic ether
12	757–748	Vibration of aromatic = C–H
13	669	Substituted benzenes

that these OCFGs would be decomposed upon heat treatment. However, at heat treatment temperature 400 °C, a further decrease in peak intensity in the 1800 ~ 1200 cm^{-1} regions had been confirmed, and the fitted peak area of ether bond, carboxyl and carbonyl decreased to 4.10, 0.06 and 0.63, respectively. This indicates that OCFGs in the 1800 ~ 1200 cm^{-1} were either decomposed or converted into more stable functional groups during heat-treated in N_2 [7, 23]. Meanwhile, the fitted peak area around 3500–3000 cm^{-1}, namely hydroxyl group, decreased continuously to 2.60 as temperature increased until 400 °C, indicating the decomposition of hydroxyl during heat

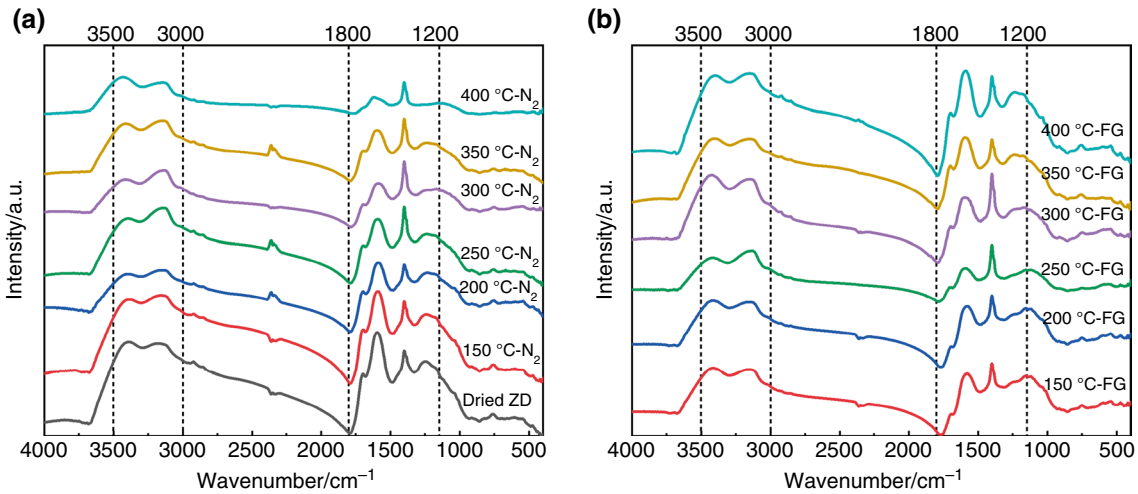

Fig.4 FTIR spectra of ZD and samples treated in **a** N_2 and **b** FG at 150–400 °C

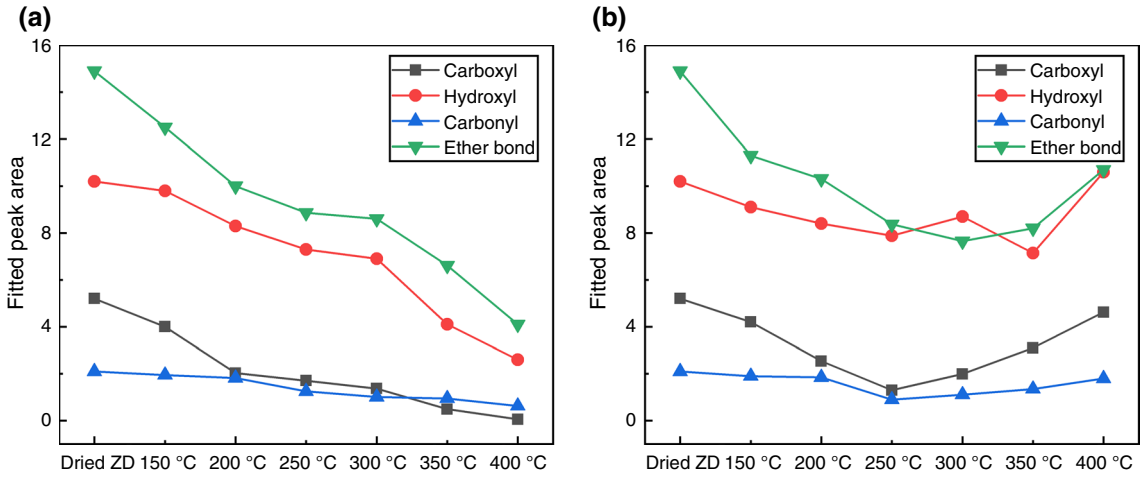

Fig. 5 Variation of OCFGs in ZDs heat-treated in **a** N_2 and **b** FG as a function of temperature

treatment. This is because the hydroxy groups are chemical active and prone to dissolve during heat treatment [4]. As for FG-treated ZDs, the contents of ether bond, carboxyl, carbonyl and hydroxyl initially decreased to 8.37, 1.30, 0.90 and 7.88 at 250 °C, but further increased to 10.71, 4.62, 1.82 and 10.71 as temperature further raised to 400 °C. This is because the presence of O_2 during heat treatment in FG, allowing for the generation of new OCFGs [4, 12]. The content of hydroxyl group in heat-treated samples even exceeded those in 105 °C dried ZD. In the presence of O_2, aliphatic chain would be oxidised and produce alkali-soluble regenerated humic acid, contributing to a dissolution in aliphatic chain and an increase in OCFGs [26, 38]. These results were consistent with the literature studies [14, 26], suggesting that the lignite would be oxidised to some extent during heat treatment in FG at 300 °C or above.

Re-adsorption characteristics

Figure 6 presents the re-adsorption behaviour of as-received ZD and those heat-treated ZDs as a function of time. When the as-received ZD was placed in the chamber at 25 °C and 65% relative humidity, the moisture content in ZD_{ar} decreased from 24.58 mass% to 17.42 mass% after 72 h, indicating that the temperature and humidity in the chamber allowed the release of moisture. On the contrary, those heat-treated ZDs in N_2, as shown in Fig. 7a, increased their moisture contents within the experimental hours. For example, ZD after heat treatment in N_2 at 150 °C had a negligible moisture content, which increased to 13.33 mass% within 24 h, and maintained at ca. 13.86 mass% in the subsequent hours. This indicates that the re-adsorption capacity of heat-treated ZDs

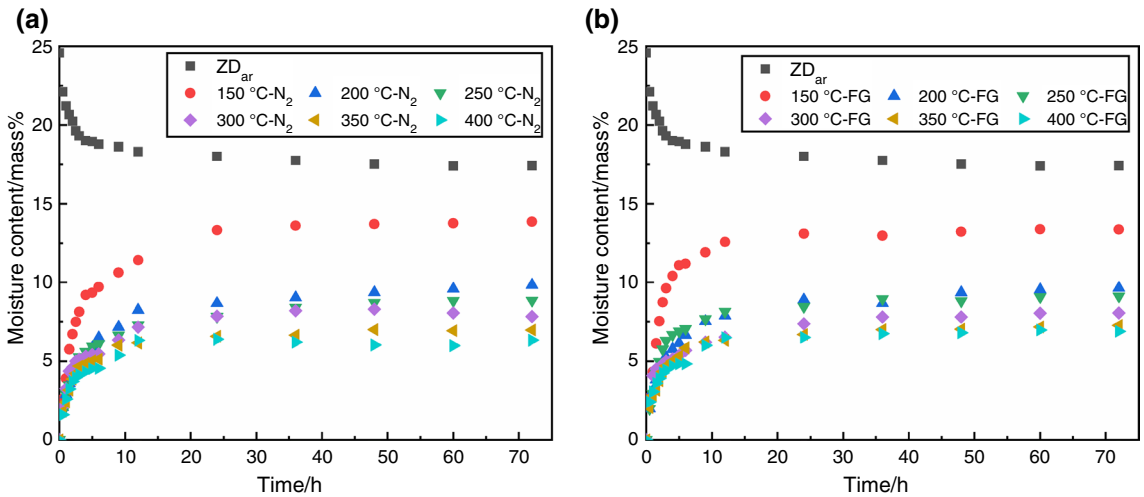

Fig. 6 Re-adsorption behaviour of ZD and samples heat-treated in **a** N_2 and **b** FG

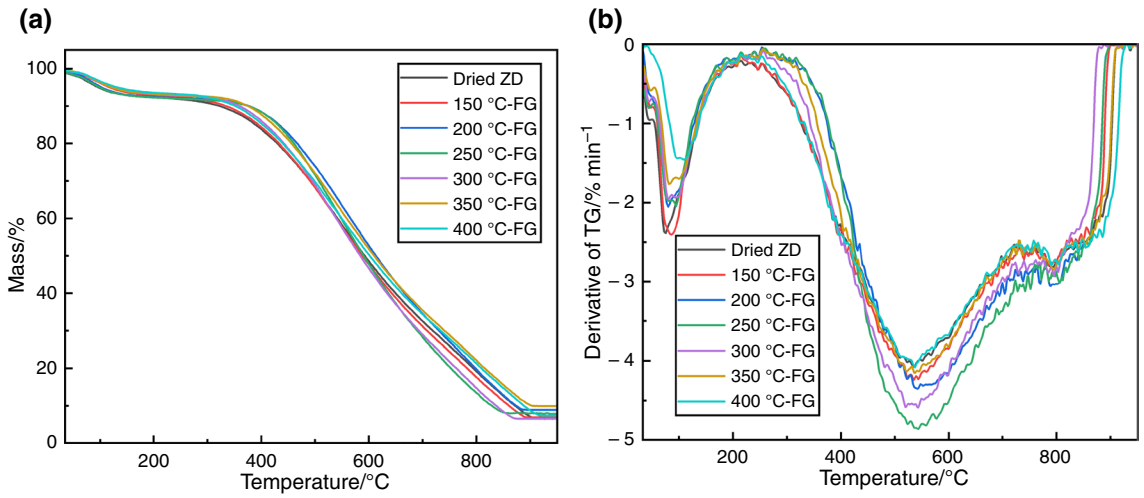

Fig. 7 **a** TG and **b** DTG curve of dried ZD and ZD heat-treated in FG during combustion in TGA

would be decreased as time proceeded, possibly due to the saturation of pores or OCFGs for water adsorption. As heat treatment temperature increased, the moister content in these ZDs heat-treated at 200–400 °C decreased to 9.83 mass%–6.32 mass%, showing a decreased hydrophilicity with heat treatment temperature. Similar trend was also applied for those samples heat-treated in FG, during which the moisture content in heat-treated samples decreased from 13.36 mass% at 150 °C to 6.88 mass% at 400 °C. This is attributed to the irreversible changes of pore structure and evolution of OCFGs as heated [4, 21]. This is also the reason why the moisture contents in heat-treated ZDs were lower than the raw ZD even after 72-h re-adsorption experiments.

It is also observed that ZDs heat-treated in FG within 150–200 °C absorbed less moisture than those treated at the same temperature but in N_2 atmosphere. For instance, the moisture content in ZD heat-treated in FG at 150 °C was about 3.7 mass% lower than that in N_2-treated ZD at 150 °C and this data reached about 2.0 mass% at 200 °C. This is because samples heat-treated in FG had a smaller D_{50} and BET special surface area in comparison with those treated in N_2, showing a severer deterioration of pore structure and thus a decreased hydrophilicity [19]. However, at 250 °C and above, ZDs treated in FG absorbed more moisture than those treated in N_2, exceeding about 2.9 mass%–8.1 mass% within the temperature range 250–400 °C. This is consistent with variation of chemical adsorption with increasing treatment temperature [41], because new OCFGs such as carboxyl and hydroxyl were generated at these temperatures, which would help re-adsorbing more moisture due to their hydrophilicity [22, 27].

Oxidisation behaviour of heat-treated ZDs

Figure 7 presents the TG-DTG curves of dried ZD and those samples heat-treated in FG. As shown in Fig. 7a, the mass loss of these samples increased to ca. 10% at 400 °C and further decreased to ca.90% at 800 °C. DTG curve showed that there were three peaks during combustion, mainly the first peak at ca. 100 °C, the second peak at ca. 540 °C and the third peak at ca. 800 °C. The first peak was mainly attributed to dehydration, which had a mass loss rate of 2.40% min^{-1} for dried ZD, but decreased to 1.46% min^{-1} for ZD treated at 400 °C, showing a decrease in mass loss rate as heat treatment temperature. This is because the capacity of water adsorption turned to be deteriorated after heat treatment, consistent with re-adsorption characteristics. As for the second peak, the maximum mass loss rate of dried ZD was 4.07% min^{-1}, which increased to 4.86% min^{-1} as heat treatment temperature increased to 250 °C, but decreased subsequently as heat treatment temperature further increased. This is attributed to physiochemical changes as discussed above since the mass loss rate was correlated to the stable macromolecular structure in upgraded lignite [10]. The third peak might be the burnout of char and decomposition of mineral matter such as carbonates, sulphates and other mineral species as well as the release of alkali metals [42], which was minimal and was not discussed further in detail.

In addition, the combustion characteristic temperatures and parameters were also calculated and the results are shown in Table 5. It is seen that dried ZD could be ignited at 364.11 °C, but those samples treated in FG had a delayed ignition temperature, and followed an order of dried ZD < 150 °C-FG < 400 °C-FG < 350 °C-FG < 300 °C-FG < 200 °C-FG < 250 °C-FG. This indicates that heat-treated

Table 5 Characteristic parameters of dried ZD and ZD heat-treated in FG during combustion in TGA

Samples	T_i/°C	T_p/°C	T_b/°C	DTG_{max} /(%·min^{-1})	FI×10^{-5} /(%·min^{-2})	CCI×10^{-7} /(%^{2}·min^{-2}·°C^{-3})
Dried ZD	364.11	534.31	884.32	4.069	3.069	1.189
150 °C-FG	378.36	536.50	871.33	4.236	2.959	1.066
200 °C-FG	410.01	542.79	867.40	4.243	2.524	0.970
250 °C-FG	411.88	543.88	851.42	4.862	2.866	1.138
300 °C-FG	391.70	543.16	843.25	4.590	2.992	1.201
350 °C-FG	386.72	539.59	873.45	4.152	2.776	0.987
400 °C-FG	381.10	537.68	885.41	4.093	2.818	0.960

ZDs are less prone to be burned than ZD [30]. This would be attributed to the physiochemical evolutions as discussed above. Likewise, T_p exhibited the same tendency as T_i, with dried ZD being the lowest (T_p = 534.31 °C) and ZD heat-treated at 250 °C being the highest (T_p = 543.88 °C). This implies that heat treatment could shift the combustion zone into a higher temperature [10]. However, the burnout temperature (T_b) presents an opposite trend, which decreased firstly to 843.25 °C for ZD treated at 300 °C, but increased to 885.41 °C for ZD treated at 400 °C, implying that ZD heat-treated at 300 °C had a better burnout capacity. As for the maximum mass loss (DTG_{max}), the dried ZD had the lowest value, followed by those samples heat-treated, indicating that the combustion reactivity was enhanced after heat treatment to a certain extent.

For the flammability index (FI) and comprehensive combustion index (CCI) as listed in Table 5, FI of heat-treated ZDs was all lower than that of dried ZD, indicating that heat treatment decreases their propensity for combustion [15]. A peak value of FI at 250 °C and 300 °C was observed, indicating a better ignition performance than other samples. This is consistent with the variation of OCFGs as temperature, since the generation of new OCFGs would benefit ignition [10]. Similar trend was also observed for CCI of these samples [43], suggesting that ZD heat-treated at 250 °C and 300 °C would have a better combustion reactivity in comparison with other treated samples.

Conclusions

The physiochemical characteristics, moisture re-adsorption behaviour and combustion characteristics of Zhundong lignite treated at different temperatures and atmospheres were experimentally investigated. Results showed that the particle sizes of ZDs heat-treated in N_2 and FG decreased at temperatures below 250 °C, with the BET special surface area decreased as a function of temperature. The oxygen content and the peak intensity of OCFGs also decreased with increasing treatment temperature in N_2, which, however, differed from ZDs treated in FG and at 250 °C and above due to generation of OCFGs such as ether bond, hydroxyl, carboxyl and carbonyl. Re-adsorption analysis confirmed that re-adsorption capacity of ZDs weakened with increasing treatment temperature, and samples treated in FG at 250 °C or above had a stronger re-adsorption capacity than that treated in N_2. Besides, due to the variation in physicochemical properties of heat-treated ZDs, the ignition temperature of FG-treated ZDs was delayed, although the combustion reactivity of these samples seems to be enhanced.

Acknowledgements This work was supported by the National Natural Science Foundation of China (Grant Number 52176101).

Declarations

Conflict of interest On behalf of all authors, the corresponding author states that there is no conflict of interest.

References

1. Duan HB, Mo JL, Fan Y, Wang SY. Achieving China's energy and climate policy targets in 2030 under multiple uncertainties. Energy Econ. 2018;70:45–60. https://doi.org/10.1016/j.eneco.2017.12.022.
2. Liu X, Li G, Xie R, Zhao Z, Cui P. A review on moisture re-adsorption of lignite treated using different drying techniques. Dry Technol. 2021. https://doi.org/10.1080/07373937.2020.1871007.
3. Liu X, Yu H, Wei L. Experimental study on the dehydration characteristics and evolution of the physicochemical structure of Xilin-Gol lignite during the dehydration process. Fuel. 2021. https://doi.org/10.1016/j.fuel.2021.120241.
4. Yu J, Tahmasebi A, Han Y, Yin F, Li X. A review on water in low rank coals: the existence, interaction with coal structure and effects on coal utilization. Fuel Process Technol. 2013;106:9–20. https://doi.org/10.1016/j.fuproc.2012.09.051.
5. Deevi SC, Suuberg EM. Physical changes accompanying drying of western United-States lignites. Fuel. 1987;66(4):454–60. https://doi.org/10.1016/0016-2361(87)90147-5.
6. Li J, Zhu M, Zhang Z, Zhang K, Shen G, Zhang D. Characterisation of ash deposits on a probe at different temperatures during combustion of a Zhundong lignite in a drop tube furnace. Fuel Process Technol. 2016;144:155–63. https://doi.org/10.1016/j.fuproc.2015.12.024.
7. Wei F, Liao J, Chang L, Han Y, Bao W. Transformation of functional groups during lignite heat-treatment and its effects

on moisture re-adsorption properties. Fuel Process Technol. 2019;192:210–9. https://doi.org/10.1016/j.fuproc.2019.04.028.
8. Zhu X, Sheng C. Evolution of the char structure of lignite under heat treatment and its influences on combustion reactivity. Energy Fuels. 2010;24(1):152–9. https://doi.org/10.1021/ef900531h.
9. Zhang Z, Zhu M, Li J, Zhang K, Shen G, Xu G, et al. Effect of heat treatment on the combustion characteristics of a lignite. J Energy Res Technol. 2019;141(7):070705–6. https://doi.org/10.1115/1.4042823.
10. Zhao H, Li Y, Song Q, Wang X, Shu X. Drying, re-adsorption characteristics, and combustion kinetics of Xilingol lignite in different atmospheres. Fuel. 2017;210:592–604. https://doi.org/10.1016/j.fuel.2017.09.011.
11. Liu S, Zhao H, Fan T, Zhou J, Liu X, Li Y, et al. Investigation on chemical structure and hydrocarbon generation potential of lignite in the different pretreatment process. Fuel. 2021. https://doi.org/10.1016/j.fuel.2021.120205.
12. Tahmasebi A, Yu J, Han Y, Yin F, Bhattacharya S, Stokie D. Study of chemical structure changes of Chinese lignite upon drying in superheated steam, microwave, and hot air. Energy Fuels. 2012;26(6):3651–60. https://doi.org/10.1021/ef300559b.
13. Zhao P, Zhong L, Zhu R, Zhao Y, Luo Z, Yang X. Drying characteristics and kinetics of Shengli lignite using different drying methods. Energy Convers Manage. 2016;120:330–7. https://doi.org/10.1016/j.enconman.2016.04.105.
14. Tahmasebi A, Yu J, Han Y, Li X. A study of chemical structure changes of Chinese lignite during fluidized-bed drying in nitrogen and air. Fuel Process Technol. 2012;101:85–93. https://doi.org/10.1016/j.fuproc.2012.04.005.
15. Yang Y, Liao J, Mo Q, Chang L, Bao W. Evolution of physical and chemical structures in lignite during dewatering process and their effects on combustion reactivity. Energy Fuels. 2019;33(5):3891–8. https://doi.org/10.1021/acs.energyfuels.8b04239.
16. Wei J, Wang M, Tang G, Akhtar MA, Xu D, Song X, et al. Advances on in-situ analysis of char structure evolution during thermochemical conversion of coal/biomass: a review. Fuel Process Technol. 2022. https://doi.org/10.1016/j.fuproc.2022.107221.
17. Hulston J, Favas G, Chaffee AL. Physico-chemical properties of Loy Yang lignite dewatered by mechanical thermal expression. Fuel. 2005;84(14–15):1940–8. https://doi.org/10.1016/j.fuel.2005.03.024.
18. Gao M, Ji P, Miao Z, Wan K, He Q, Xue S, et al. Pore structure evolution and fractal characteristics of Zhaotong lignite during drying. Fuel. 2020. https://doi.org/10.1016/j.fuel.2020.117309.
19. Salmas CE, Tsetsekou AH, Hatzilyberis KS, Androutsopoulos GP. Evolution lignite mesopore structure during drying. Effect of temperature and heating time. Dry Technol. 2001;19(1):35–64. https://doi.org/10.1081/DRT-100001351.
20. Feng X, Zhang C, Tan P, Zhang X, Fang Q, Chen G. Experimental study of the physicochemical structure and moisture readsorption characteristics of Zhaotong lignite after hydrothermal and thermal upgrading. Fuel. 2016;185:112–21. https://doi.org/10.1016/j.fuel.2016.07.101.
21. Zhang Y, Jing X, Jing K, Chang L, Bao W. Study on the pore structure and oxygen-containing functional groups devoting to the hydrophilic force of dewatered lignite. Appl Surf Sci. 2015;324:90–8. https://doi.org/10.1016/j.apsusc.2014.10.126.
22. Li Z, Zhang Y, Jing X, Zhang Y, Chang L. Insight into the intrinsic reaction of brown coal oxidation at low temperature: differential scanning calorimetry study. Fuel Process Technol. 2016;147:64–70. https://doi.org/10.1016/j.fuproc.2015.07.030.
23. Lin X, Wang C, Ideta K, Miyawaki J, Nishiyama Y, Wang Y, et al. Insights into the functional group transformation of a Chinese brown coal during slow pyrolysis by combining various experiments. Fuel. 2014;118:257–64. https://doi.org/10.1016/j.fuel.2013.10.081.
24. Tahmasebi A, Yu J, Bhattacharya S. Chemical structure changes accompanying fluidized-bed drying of Victorian brown coals in superheated steam, nitrogen, and hot air. Energy Fuels. 2012;27(1):154–66. https://doi.org/10.1021/ef3016443.
25. Zhao Y, Wang Z, Zhao G, Sun R. Effects of upgrading treatment on the physicochemical structure, moisture re-adsorption ability, and NOx emission characteristic of lignite particles. Energy Fuels. 2019;33(5):4070–8. https://doi.org/10.1021/acs.energyfuels.9b00306.
26. Lu W, Li J, Li J, He Q, Hao W, Li Z. Oxidative kinetic characteristics of dried soaked coal and its related spontaneous combustion mechanism. Fuel. 2021. https://doi.org/10.1016/j.fuel.2021.121626.
27. Rish SK, Tahmasebi A, Yu J. A DSC study on the impact of low-temperature oxidation on the behavior and drying of water in lignite. J Therm Anal Calorim. 2019;139(6):3507–17. https://doi.org/10.1007/s10973-019-08749-w.
28. Suuberg EM, Otake Y, Yun Y, Deevi SC. Role of moisture in coal structure and the effects of drying upon the accessibility of coal structure. Energy Fuels. 1993;7(3):384–92.
29. Liu X, Hirajima T, Nonaka M, Sasaki K. Effects of hydrothermal treatment coupled with mechanical expression on combustion performance of Loy Yang lignite. J Therm Anal Calorim. 2016;126(3):1925–35. https://doi.org/10.1007/s10973-016-5692-3.
30. Sun M, Ning X, Zhang J, Li K, Tang Q, Liu Z, et al. Combustion kinetics and structural features of bituminous coal before and after modification process. J Therm Anal Calorim. 2017;131(2):983–92. https://doi.org/10.1007/s10973-017-6709-2.
31. Li Y, Chen MQ, Huang YW. Evaluation on the non-isothermal combustion kinetics of lignite and sewage sludge through microwave pretreatment. J Therm Anal Calorim. 2019;141(3):1165–72. https://doi.org/10.1007/s10973-019-09107-6.
32. Cao W, Cao W, Peng Y, Qiu S, Miao N, Pan F. Experimental study on the combustion sensitivity parameters and pre-combusted changes in functional groups of lignite coal dust. Powder Technol. 2015;283:512–8. https://doi.org/10.1016/j.powtec.2015.06.025.
33. Li J, Zhu M, Zhang Z, Zhang K, Shen G, Zhang D. Effect of coal blending and ashing temperature on ash sintering and fusion characteristics during combustion of Zhundong lignite. Fuel. 2017;195(Supplement C):131–42. https://doi.org/10.1016/j.fuel.2017.01.064.
34. Nie Y, Deng M, Shan M, Yang X. Evaluating the impact of wood sawdust and peanut shell mixing ratio on co-combustion performance. Fuel. 2022. https://doi.org/10.1016/j.fuel.2022.124667.
35. Wu J, Wang B, Cheng F. Thermal and kinetic characteristics of combustion of coal sludge. J Therm Anal Calorim. 2017;129(3):1899–909. https://doi.org/10.1007/s10973-017-6341-1.
36. Shi L, Cheng X, Liu Q, Liu Z. Reaction of volatiles from a coal and various organic compounds during co-pyrolysis in a TG-MS system. Part 1. Reaction of volatiles in the void space between particles. Fuel. 2018;213:37–47. https://doi.org/10.1016/j.fuel.2017.10.083.
37. Androutsopoulos GP, Linardos TJ. Effects of drying upon lignite macro-pore structure. Powder Technol. 1986;47(1):9–15. https://doi.org/10.1016/0032-5910(86)80002-X.
38. Calemma V, Iwanski P, Rausa R, Girardi E. Changes in coal structure accompanying the formation of regenerated humic acids during air oxidation. Fuel. 1994;73(5):700–7. https://doi.org/10.1016/0016-2361(94)90012-4.
39. Hu B, Xie W-L, Li H, Li K, Lu Q, Yang Y-P. On the mechanism of xylan pyrolysis by combined experimental and computational approaches. Proc Combust Inst. 2021;38(3):4215–23. https://doi.org/10.1016/j.proci.2020.06.172.

40. Meng D, Yue C, Wang T, Chen X. Evolution of carbon structure and functional group during Shenmu lump coal pyrolysis. Fuel. 2021. https://doi.org/10.1016/j.fuel.2020.119538.
41. Jing X, Jing K, Li Z, Liu X, Zhang Y, Chang L, et al. Thermal effect during moisture re-adsorption of dewatered lignite. J Therm Anal Calorim. 2014;119(3):2187–94. https://doi.org/10.1007/s10973-014-4299-9.
42. Wang X, Ruan R, Yang T, Adeosun A, Zhang L, Wei B, et al. Sulfate removal by kaolin addition to address fouling in a full-scale furnace burning high-alkaline Zhundong coal. Energy Fuels. 2017;31(11):12823–30. https://doi.org/10.1021/acs.energyfuels.7b02099.
43. Wzorek M, Junga R, Yilmaz E, Bozhenko B. Thermal decomposition of olive-mill byproducts: a TG-FTIR approach. Energies. 2021. https://doi.org/10.3390/en14144123.